

Acceleration of relativistic beams using laser-generated terahertz pulses

Morgan T. Hibberd^{1,2}, Alisa L. Healy^{1,3}, Daniel S. Lake^{1,4}, Vasileios Georgiadis^{1,2}, Elliott J. H. Smith^{1,2}, Oliver J. Finlay^{1,4}, Thomas H. Pacey^{1,5}, James K. Jones^{1,5}, Yuri Saveliev^{1,5}, David A. Walsh^{1,5}, Edward W. Snedden^{1,5}, Robert B. Appleby^{1,2}, Graeme Burt^{1,3}, Darren M. Graham^{1,2}, and Steven P. Jamison^{*1,4}

¹The Cockcroft Institute, Sci-Tech Daresbury, Keckwick Lane, Daresbury, Warrington WA4 4AD, UK.

²Department of Physics and Astronomy & Photon Science Institute, The University of Manchester, Oxford Road, Manchester M13 9PL, UK.

³Department of Engineering, Lancaster University, Bailrigg, Lancaster LA1 4YW, UK.

⁴Department of Physics, Lancaster University, Bailrigg, Lancaster LA1 4YB, UK.

⁵Accelerator Science and Technology Centre, Science and Technology Facilities Council, Sci-Tech Daresbury, Keckwick Lane, Daresbury, Warrington WA4 4AD, UK.

Particle accelerators driven by laser-generated terahertz (THz) pulses promise unprecedented control over the energy-time phase-space of particle bunches compared with conventional radio-frequency technology. Here, we make a breakthrough achievement by demonstrating for the first time, acceleration of a relativistic electron beam in a THz-driven linear accelerator. Narrowband THz pulses were tuned to the phase-velocity-matched operating frequency of a rectangular dielectric-lined waveguide for extended collinear interaction with 35 MeV, 60 pC electron bunches, imparting multi-cycle energy modulation to chirped (6 ps) bunches and injection-phase-dependent energy gain (up to 10 keV) to sub-cycle (2 ps) bunches. These proof-of-principle results establish a route to whole-bunch linear acceleration of sub-picosecond particle beams, directly applicable to scaled-up and multi-staged concepts capable of preserving beam quality, thus marking a key milestone for future THz-driven acceleration of relativistic beams.

Laser-driven acceleration in dielectric structures is a well-established approach¹⁻⁴ that may hold the key to overcoming the technological limitations of conventional particle accelerators. However, injecting sub-femtosecond particle bunches into optical-frequency accelerating structures to achieve whole-bunch acceleration remains a significant challenge. A promising solution is to down-convert the laser excitation into the terahertz (THz) frequency regime, where THz pulses with electric fields exceeding 1 GV/m have recently been reported⁵. With experimental demonstrations of THz-driven acceleration, compression and streaking with low-energy (sub-100 keV) electron beams⁶⁻⁹, operation at relativistic beam energies is now essential to realise the full potential of THz-driven structures. Here, we present results from the Compact Linear Accelerator for Research and Applications (CLARA) test facility at Daresbury Laboratory, reporting the first THz-driven linear acceleration of a relativistic electron beam. A dielectric-lined waveguide (DLW) was collinearly excited by phase-velocity-matched, polarisation-tailored, narrowband THz pulses to successfully accelerate 35 MeV electron bunches with charges of up to 60 pC. This proof-of-principle demon-

stration is directly applicable to both scaled-up and multi-staged acceleration, marking a key milestone in the development of future high-energy, high-charge THz-driven accelerators.

The need to overcome the electrical breakdown threshold currently limiting the achievable accelerating field gradients of radio-frequency (RF)-based accelerators has led to the development of both laser-driven¹⁰ and beam-driven¹¹ acceleration schemes. With the laser-based schemes also capable of exploiting the femtosecond timing synchronisation to laser-generated electron bunches, this has resulted in developments in the optical-infrared regime exploring free-space acceleration^{12,13}, laser-driven plasma wakefield acceleration¹⁴⁻¹⁶ and dielectric laser acceleration (DLA) in scalable, phase-matched dielectric microstructures¹⁻⁴. DLA schemes face significant challenges using sub-micron optical wavelengths to drive the structures, which put extreme tolerances on fabrication and bunch timing jitter, while also limiting the amount of bunch charge that can be supported.

Laser-generated THz radiation exists in the ideal millimeter-scale wavelength regime, making structure

fabrication simpler but most importantly providing picosecond pulse cycle lengths well-suited for flexible manipulation of sub-picosecond electron bunches with pC-level charge. In recent years, numerous THz-electron interactions have been explored, including acceleration using a dielectric-lined waveguide⁶, electron emission off metal nanotips¹⁷, streaking and bunch compression both with metallic resonators⁷ and by driving dielectric tubes with circularly polarized THz pulses¹⁸, and the development of novel phase-matching schemes for increased interaction length based on segmented waveguides⁹, near-field travelling waves¹⁹ and inverse free-electron laser (IFEL)-driven microbunching²⁰. The wide scope of work demonstrates the drive towards understanding and exploiting the unique capabilities of THz pulses through structure-mediated interactions for unparalleled control over the spatial, temporal and energy properties of electron beams.

Concept and implementation

Here, we demonstrate linear acceleration of relativistic 35 MeV electron beams using a DLW structure driven by laser-generated THz radiation. For the first time, we implement phase-velocity matching of the THz field with the propagating electron bunch ($v_p = v_e = 0.9999c$), making extended field-driven interaction possible. However, in contrast to sub-relativistic experiments where the group and phase velocity of the field in the mediating structure differ by only a small margin⁶, at relativistic energies with the required phase velocity close to c , the group velocity is inherently lower by nearly a factor of 2 (see Supplementary Information). We mitigate this group velocity walk-off through generation of a narrow-band THz pulse with multiple cycles, thereby increasing the pulse duration and facilitating an extended interaction length. The THz pulse is further manipulated into a quasi-TEM₀₁ polarisation state to provide the necessary coupling to the longitudinal accelerating mode of the DLW structure for collinear acceleration, with an accelerating gradient of 2 MV/m achieved using modest THz pulse energies. The gradient demonstrated is an order of magnitude higher than recent IFEL-coupled acceleration experiments on relativistic electron beams²⁰, and unlike the IFEL interaction, which scales inversely with beam energy, our gradient is independent of electron energy and is therefore directly applicable for scaling to future high-energy, relativistic acceleration. In our experiment, the resulting peak THz-driven acceleration of long-duration (6 ps FWHM) electron bunches was determined from the modulation of the energy spectrum, which also revealed quantitatively the time-energy phase-space of the bunch. Electron bunches with shorter duration (2 ps FWHM) comparable to the period of the THz pulse, are shown to undergo preferential acceleration or deceleration dependent on the timing of electron

bunch injection relative to the phase of the THz pulse. Given the DLW structure enabled the transmission and acceleration of bunch charges up to 60 pC, over 3 orders of magnitude higher than in previous sub-relativistic acceleration experiments⁹, our proof-of-principle results demonstrate the route to whole-bunch acceleration of high-charge, sub-picosecond relativistic particle beams.

The THz-electron beam interaction arrangement is shown schematically in Fig. 1. Relativistic 35 MeV electron bunches with configurable charge, bunch duration and chirp were delivered to the experiment by the CLARA accelerator²¹. Magnetic quadrupole triplets provided electron bunch transverse control for coupling into the DLW and for optimising the energy resolution of the dipole spectrometer. Frequency-tunable, narrow-band (100 GHz FWHM) THz pulses with approximately 2 μ J energy were generated through chirped-pulse beating^{22,23} in a lithium niobate crystal (see Methods). A quasi-TEM₀₁ mode was generated by a phase-shifter plate providing a $\lambda/2$ shear and an effective polarity inversion^{24,25} along the horizontal midline of the THz beam, which is revealed by the electro-optic sampling measurements in Fig. 1a. The DLW structure was a rectangular copper waveguide lined at the top and bottom with 60 μ m-thick fused-quartz, leaving a vertical 575 μ m-thick free-space aperture for electron beam propagation. An integrated linearly-tapered horn was used to couple the quasi-TEM₀₁ mode of the THz beam into the accelerating longitudinal section magnetic (LSM₁₁) mode²⁶ of the DLW, which was designed for phase-velocity matching with the electron bunch at an operating frequency of 0.4 THz (see Supplementary Information).

Multi-cycle energy modulation

The effect of THz-driven acceleration on an approximately linear chirped, 6 ps FWHM electron bunch is demonstrated in Fig. 2, with single-shot energy spectra shown for THz off (Fig. 2a) and THz on (Fig. 2b) following temporal overlap of the THz pulse with an electron bunch in the DLW. The difference between the energy spectra in Fig. 2c reveals an energy modulation shown in Fig. 2d, with up to 90% modulation strength, defined as the peak-to-peak amplitude of the modulation normalised to the amplitude of the unmodulated (THz off) spectrum (Methods). The modulation arises from the temporally sinusoidal energy gain induced by the multi-cycle THz pulse on the initial longitudinal phase-space distribution of the electron bunch. With sufficiently large energy gain (and loss), it was possible to impose a significant change in the temporally localised chirp of the bunch, resulting in a non-sinusoidal spectral density. This behavior can be observed from the measured modulation in Fig. 2d, with the peaks occurring where the THz-induced modulation flattened the local chirp to zero.

The peak THz acceleration (δE_{THz}) was determined from comparison of the measured single-shot modulation with a calculation of a sinusoidal THz-driven modulation imposed on a model electron bunch. The spatial resolution limitation of the spectrometer, arising from beam emittance and uncorrelated time-slice energy spread served to reduce the observed modulation strength, and were included in the modelling as an effective energy spread (δE_{eff}). From particle tracking modelling, neither the slice energy spread or emittance are subject to significant growth, either in our experiments or in future higher energy accelerators (see Methods, Supplementary information). Simultaneous optimisation of peak THz acceleration, effective energy spread and chirp (both linear and cubic) provided the modelled modulation shown in Fig. 2d, with a final value of $\delta E_{\text{THz}} = 8.8$ keV obtained. With an effective interaction length limited to approximately 4.3 mm by group-velocity walk-off and the THz pulse duration (see Supplementary Information), an average acceleration gradient of 2 MV/m was determined. The model also predicted a value of $\delta E_{\text{eff}} = 7.9$ keV, and both linear and cubic chirp components of 47.3 keV/ps and 0.4 keV/ps³, respectively.

To further support the above calculation of the acceleration gradient, an independent and direct measurement of the phase-space distribution was obtained from the known THz period $\tau = 2.5$ ps (0.4 THz) and the measured energy modulation period $\Delta E(E)$. The experimentally determined chirp of the electron beam ($\Delta E(E)/\tau$) shown in Fig. 2f, was obtained from 100 successive shots using the same electron bunch configuration from Fig. 2a-d. The quadratic dependence indicates the presence of a third-order chirp component, in good agreement with the modelled chirp (solid blue line in Fig. 2f), obtained independently from the single-shot analysis of Fig. 2d. The measured linear chirp (47.5 keV/ps) was of comparable magnitude with the value (53 keV/ps) predicted by beam dynamics simulations. However, the degree of phase-space curvature implied by the cubic chirp, revealed from the experimental and modelled data in Fig. 2f, was not expected from the space-charge dominated beam dynamics of the CLARA electron gun. This direct experimental measurement of the time-energy phase-space distribution of a relativistic electron beam is often inaccessible, requiring RF-driven transverse deflecting structures and dedicated electron beam optics²⁷. These measurements therefore demonstrate the advantage of THz-driven accelerating structures for both manipulating and exploring the picosecond temporal structure of high-energy electron beams.

Relativistic phase-velocity matching

The role of the DLW structure in matching the THz phase-velocity (v_p) and electron bunch velocity (v_e) was explored through the frequency-dependent interaction strength, as shown in Fig. 3. The DLW was designed with $v_p = v_e = 0.9999c$ at 0.40 THz, and correspondingly the maximum interaction (modulation strength) was observed at this frequency. The length-integrated interaction strength was modelled using the calculated DLW dispersion for a 100 GHz FWHM bandwidth THz pulse. The width of the resonant frequency response was attributable to both the spectral width of the THz pulse and the temporal walk-off between the THz pulse envelope and the electron bunch. For the 7 ps FWHM duration THz pulses used here, the group-velocity walk-off limited the effective interaction length to 4.3 mm (see Supplementary Information). The use of narrower bandwidth THz pulses with longer duration will proportionally increase the effective interaction length and could be achieved by either stretching the laser pulses in the chirped pulse beating setup, or by implementing periodically-poled lithium niobate sources, which have been shown to produce THz pulses exceeding 100 ps²⁸. Together with multi-staging of structures and sources, as in conventional RF linear accelerators, we have a route for scaling the length of future THz driven accelerators. Over the THz frequency range investigated, the modulation period imposed on the bunch was dominated by the interaction efficiency and was observed to remain approximately constant at the value (165 ± 10 keV) obtained at the resonant frequency of 0.4 THz, as shown in Fig. 3.

Sub-cycle acceleration

Compared with optical-frequency DLA structures, THz-driven acceleration offers the potential for injection of an electron bunch into a single half-cycle (or accelerating bucket) of the THz electric field. To demonstrate this, the CLARA accelerator was configured to provide an electron beam with low time-integrated energy spread and an independently measured bunch duration of approximately 2 ps FWHM (see Methods). With a duration comparable to the THz period, preferential acceleration or deceleration of the bunch was achievable, dependent on the bunch injection timing relative to the phase of the THz pulse. Single-shot electron spectra measured in this configuration are shown in Fig. 4a, with observed spectral profiles ranging from symmetric energy spreading to either asymmetric acceleration or deceleration. The maximum measured energy spread FWHM doubled from 21 keV (THz off) to 42 keV (THz on) for the symmetric spreading observed at π injection phase. This symmetric modulation is similar to that observed in optical-frequency DLA structures¹, where the bunch

duration covers many cycles of the optical excitation pulse. However, the asymmetric energy spread observed in Fig. 4a was only achievable through a whole-bunch charge-density asymmetry with respect to the THz oscillation period. A model distribution (see Fig. 4d) of the low energy spread, short-duration electron bunch was based on particle tracking simulations, with a small residual chirp expected from this accelerator configuration (see Methods). This distribution was then modulated at the THz frequency (see Fig. 4e) over the full 2π range of injection phases to give the modelled energy spectra in Fig. 4b and c. Optimal matching to the measured spectra was achieved using an effective energy spread (see Methods) of $\delta E_{\text{eff}} = 5.9$ keV, residual linear chirp of 7.8 keV/ps and a peak THz-driven acceleration of $\delta E_{\text{THz}} = 10.0$ keV, consistent with the value obtained from the multi-cycle modulation analysis in Fig. 2. The experimentally observed and modelled asymmetric acceleration is unambiguous evidence of predominant injection into a single half-cycle of the THz pulse.

Conclusions and outlook

In summary, we have successfully demonstrated the linear acceleration of relativistic electron beams using a dielectric-lined waveguide driven by narrowband, frequency-tunable, polarisation-tailored THz pulses. We were able to exploit multi-cycle THz-driven modulation to manipulate the electron energy spectra and determine the bunch chirp, while also observe preferential acceleration of bunches with duration comparable to a single cycle of the THz pulse. Our results were achieved using electron bunches with up to 3 orders of magnitude higher charge and energy than previously reported, exploiting an accelerating structure that we have shown through simulations (see Supplementary Information) to preserve the transverse beam quality in both this experiment and in a future high-energy accelerator. Furthermore, with the implementation of narrower bandwidth²⁸ and higher energy⁵ THz sources, our proof-of-principle approach is amenable to both scaled-up and multi-staged acceleration, establishing a key milestone for future THz-driven acceleration of high-energy, high-charge and high-quality relativistic beams.

Methods

Electron beam

This experiment was carried out at the CLARA research facility at Daresbury Laboratory. Electron bunches were generated from a copper cathode by 266 nm, 2 ps FWHM photoinjector laser pulses at a repetition rate of 10 Hz. The bunches were initially accelerated in a 3 GHz RF gun to 5 MeV and then transported to a linac for further acceleration up to 35 MeV. The relativistic electron

bunches were transported to an experimental user station using a magnetic dog-leg, which in combination with the linac, allowed for manipulation of the longitudinal phase-space of the beam. Two main accelerator configurations were used for this experiment; a long bunch with large energy spread (Fig. 2), and a shorter bunch with low energy spread (Fig. 4). For the long-bunch configuration, the bunch duration and chirp were determined directly from the THz-driven modulation data (Fig. 2 and main text) and were broadly consistent with beam dynamics simulations performed using the code Elegant. For the short-bunch configuration, a bunch duration of 2 ps FWHM, measured by the method of RF zero-phasing, was used directly in the model analysis of Fig. 4. The linear chirp of 7.8 keV/ps was in line with accelerator tuning and space-charge expectations. In the experimental user station, the electron beam was transversely focused into the DLW by an upstream quadrupole triplet (see Fig. 1) to a RMS transverse size of 100 μm . After transmission through the DLW a downstream quadrupole triplet was used for matching the beam into the energy spectrometer and minimising the horizontal β -function.

Laser systems

The experiment was performed using a customised terawatt (TW) laser system²⁹, capable of producing up to 800 mJ laser pulses at 10 Hz with a centre wavelength of 800 nm and Fourier-limited pulse duration of 60 fs. The TW system comprised of a Ti:sapphire oscillator (Micra, Coherent) producing 800 nm, 30 fs, 4 nJ pulses at 83 MHz, which were stretched to approximately 150 ps and used to seed a Ti:sapphire regenerative amplifier (Legend, Coherent) providing 800 nm, 50 fs (Fourier-limited), 1 mJ pulses at 1 kHz. The uncompressed output of the regenerative amplifier was routed through a multi-pass Ti:sapphire amplifier (MPA), where two frequency-doubled Nd:YAG lasers (Powerlite II, Continuum) producing 532 nm, 10 ns, 1.5 J pulses at 10 Hz provided the pump energy for amplification, which following re-compression to 60 fs resulted in TW peak powers. For the experiment, a laser pulse energy of approximately 50 mJ was delivered to the electron beam experimental user station through an evacuated beam transport line.

Terahertz generation

Narrowband THz pulses were generated using a chirped-pulse beating scheme combined with tilted pulse-front pumping of a 0.6% MgO-doped stoichiometric lithium niobate (LiNbO_3) crystal. Chirped-pulse beating was achieved by adjusting the TW grating-pair compressor to chirp the input laser pulse and a Michelson interferometer was used to generate THz radiation at the beat frequency set by the interferometric combination of the two chirped laser pulses in the LiNbO_3 crystal. With an input chirped pulse duration of approximately 12 ps

FWHM, THz pulses with centre frequency of 0.40 THz and bandwidth of 100 GHz were generated. The tilted pulse-front was achieved using a diffraction grating with groove density of 1700 mm^{-1} , incident angle of 31.2° and diffracted angle of 57.5° . A 4f-lens configuration consisting of two cylindrical lenses of 130 mm and 75 mm focal length was used to image the pulse-front tilt in the LiNbO_3 crystal. The resulting pump $1/e^2$ spot size on the LiNbO_3 crystal was 5 mm x 10 mm and with a pump pulse energy of 18 mJ, THz pulses with an approximate energy of $2.1 \mu\text{J}$ were measured at the crystal surface using a pyroelectric detector (THZ-I-BNC, Gentec). The THz radiation was collected by a 90° off-axis parabolic mirror (OPM) of 152.4 mm focal length and routed by silver mirrors into a vacuum chamber through a quartz window. Focusing of the THz radiation was achieved using a 228.6 mm focal length OPM combined with a 100 mm focal length TPX lens, resulting in a $1/e^2$ spot size of approximately 3 mm at the waveguide coupler entrance and a measured THz energy of approximately $0.79 \mu\text{J}$. A small fraction (5%) of the chirped 12 ps laser beam was re-compressed back to 60 fs FWHM by a second grating-pair compressor and focused on to a 500 μm -thick, (110)-cut ZnTe crystal in a back-reflection geometry for electro-optic sampling measurements of the THz electric field at the entrance of the waveguide. For generating the quasi- TEM_{01} THz mode, a 40 mm-diameter polytetrafluoroethylene (PTFE) phase-shifter plate was made with a thickness difference between the top and bottom halves of approximately 800 μm .

Synchronisation

The ultrafast 83 MHz Ti:sapphire oscillator (at the front end of the TW laser system) was synchronised to a reference frequency from the CLARA master clock using a commercial phase-lock loop electronics module (Synchrolock, Coherent). The master clock was derived from the Ti:sapphire oscillator (Element, Spectra-Physics) integrated into the CLARA photoinjector laser system. The RMS timing jitter between the two oscillators was measured to be approximately 100 fs. Temporal overlap of the THz pulse with the electron bunch at the DLW entrance was achieved using a Schottky diode, which detected both the driving THz pulse directly and the coherent transition radiation (CTR) generated by the 35 MeV electron beam incident on a vacuum-metal interface inserted into the beam path. Phase adjustments of the commercial phase-lock loop electronics module were used for coarse control, after which a mechanical delay stage (with range of 1 ns and step-size of 33 fs) on the THz beam line was used for fine control of the temporal overlap.

Waveguide structure

The waveguide design was a hollow, rectangular copper structure lined at the top and bottom with 60 μm -thick fused quartz (using a glycol phthalate adhesive), leaving a 575 μm -thick free-space aperture of 30 mm length and 1.2 mm width for electron beam propagation (see Supplementary Information). To maximise coupling of the THz radiation into the accelerating mode of the DLW, a tapered horn structure was fabricated with an entrance aperture of 3.25 mm by 3.18 mm and length of 23 mm. A 45° aluminium mirror with a 400 μm aperture aligned to the DLW was used to spatially overlap the incident reflected THz radiation with the transmitted electron beam. The overall DLW/coupler/mirror structure was located on a motorised 5-axis translation stage providing fine control over the positioning and tilt angle for optimisation of the THz and electron beam transmission.

Modelling

Analogous to the definition of visibility of fringes in optical interferometry, the electron energy spectrum modulation was characterised by a modulation depth (or strength), defined as $(\rho_{\text{max}} - \rho_{\text{min}})/\rho_0$, where ρ_{max} and ρ_{min} are the maximum and minimum spectral densities in a modulation period, and ρ_0 is the corresponding spectral density in the absence of THz-induced modulation. An effective energy spread (δE_{eff}) was used in the model analyses to describe the spatial resolution (σ_{rms}) of the electron spectrometer and was related to the spectrometer dispersion (D), uncorrelated time-slice energy spread (δE_{uncorr}), beam emittance (ϵ) and beam optical β -function by $\delta E_{\text{eff}} = \sigma_{\text{rms}}/D = \sqrt{\delta E_{\text{uncorr}}^2 + \epsilon^2 \beta^2/D^2}$, where σ_{rms} was determined to be 270 μm and 200 μm for the beam conditions used in the measurements of Fig. 2 and Fig. 4, respectively. The modelled frequency-dependent energy gain shown in Fig. 3 was calculated using $\delta E_{\text{gain}} = q \int_0^L E_z(z, t = (z - z_0)/v_e) dz$ for particles injected with phase-offset z_0 . The propagating field $E_z(z, t)$ at the particle position was calculated over the DLW length (L) from the frequency-domain spectrum of the THz pulse and the frequency-dependent propagation wavevector for the DLW.

Data availability

The data associated with the paper are openly available from the Zenodo data repository at: <http://doi.org/10.5281/zenodo.3903506>.

References

1. Peralta, E. A. et al. Demonstration of electron acceleration in a laser-driven dielectric microstructure.

- Nature* **503**, 91–94 (2013).
2. Breuer, J. & Hommelhoff, P. Laser-based acceleration of nonrelativistic electrons at a dielectric structure. *Phys. Rev. Lett.* **111**, 134803 (2013).
 3. Naranjo, B., Valloni, A., Putterman, S. & Rosenzweig, J. B. Stable charged-particle acceleration and focusing in a laser accelerator using spatial harmonics. *Phys. Rev. Lett.* **109**, 164803 (2012).
 4. Niedermayer, U., Egenolf, T., Boine-Frankenheim, O. & Hommelhoff, P. Alternating-phase focusing for dielectric-laser acceleration *Phys. Rev. Lett.* **121**, 214801 (2018).
 5. Liao, G. et al. Multimillijoule coherent terahertz bursts from picosecond laser-irradiated metal foils. *Proc. Natl Acad. Sci. USA* **116**, 3994–3999 (2019).
 6. Nanni, E. A. et al. Terahertz-driven linear electron acceleration. *Nat. Commun.* **6**, 8486 (2015).
 7. Kealhofer, C. et al. All-optical control and metrology of electron pulses. *Science* **352**, 429–433 (2016).
 8. Huang, W. R. et al. Terahertz-driven, all-optical electron gun. *Optica* **3**, 1209–1212 (2016).
 9. Zhang, D. et al. Segmented terahertz electron accelerator and manipulator (STEAM). *Nat. Photon.* **12**, 336–342 (2018).
 10. England, R. J. et al. Dielectric laser accelerators. *Rev. Mod. Phys.* **86**, 1337–1389 (2014).
 11. O’Shea, B. D. et al. Observation of acceleration and deceleration in gigaelectron-volt-per-metre gradient dielectric wakefield accelerators. *Nat. Commun.* **7**, 12763 (2016).
 12. Carbajo, S. et al. Direct longitudinal laser acceleration of electrons in free space. *Phys. Rev. Accel. Beams* **19**, 021303 (2016).
 13. Thévenet, M. et al. Vacuum laser acceleration of relativistic electrons using plasma mirror injectors *Nat. Phys.* **12**, 355–360 (2016).
 14. Faure, J. et al. A laser–plasma accelerator producing monoenergetic electron beams. *Nature* **431**, 541–544 (2004).
 15. Leemans, W. P. et al. Multi-GeV electron beams from capillary-discharge-guided subpetawatt laser pulses in the self-trapping regime. *Phys. Rev. Lett.* **113**, 245002 (2014).
 16. Guénot, D. et al. Relativistic electron beams driven by kHz single-cycle light pulses. *Nat. Photon.* **11**, 293–296 (2017).
 17. Li, S. & Jones, R. R. High-energy electron emission from metallic nano-tips driven by intense single-cycle terahertz pulses. *Nat. Commun.* **7**, 13405 (2016).
 18. Zhao, L. et al. Terahertz oscilloscope for recording time information of ultrashort electron beams. *Phys. Rev. Lett.* **122**, 144801 (2019).
 19. Walsh, D. A. et al. Demonstration of sub-luminal propagation of single-cycle terahertz pulses for particle acceleration. *Nat. Commun.* **8**, 421 (2017).
 20. Curry, E., Fabbri, S., Maxson, J., Musumeci, P. & Gover, A. Meter-scale terahertz-driven acceleration of a relativistic beam. *Phys. Rev. Lett.* **120**, 094801 (2018).
 21. Clarke, J. A. et al. CLARA conceptual design report. *J. Instrum.* **9**, T05001 (2014).
 22. Chen, Z., Zhou, X., Werley, C. A. & Nelson, K. A. Generation of high power tunable multicycle terahertz pulses. *Appl. Phys. Lett.* **99**, 071102 (2011).
 23. Uchida, K. et al. Time-resolved observation of coherent excitonic nonlinear response with a table-top narrowband THz pulse wave *Appl. Phys. Lett.* **107**, 221106 (2015).
 24. Cliffe, M. J., Graham, D. M. & Jamison, S. P. Longitudinally polarized single-cycle terahertz pulses generated with high electric field strengths. *Appl. Phys. Lett.* **108**, 221102 (2016).
 25. Hibberd, M. T., Lake, D. S., Johansson, N. A. B., Thomson, T., Jamison, S. P. & Graham, D. M. Magnetic-field tailoring of the terahertz polarization emitted from a spintronic source. *Appl. Phys. Lett.* **114**, 031101 (2019).
 26. Healy, A. L., Burt, G. & Jamison, S. P. Electron-terahertz interaction in dielectric-lined waveguide structures for electron manipulation. *Nucl. Instr. Meth. Phys. Res. A* **909**, 199–203 (2018).
 27. Röhrs, M., Gerth, C., Schlarb, H., Schmidt, B. & Schmäser, P. Time-resolved electron beam phase space tomography at a soft x-ray free-electron laser *Phys. Rev. ST Accel. Beams* **12**, 050704 (2009).
 28. Ahr, F. et al. Narrowband terahertz generation with chirped-and-delayed laser pulses in periodically poled lithium niobate *Opt. Lett.* **42**, 2118–2121 (2017).
 29. Priebe, G. et al. Inverse Compton backscattering source driven by the multi-10 TW laser installed at Daresbury. *Laser Part. Beams* **26**, 649–660 (2008).

30. Snively, E. C. et al. Femtosecond Compression Dynamics and Timing Jitter Suppression in a THz-driven Electron Bunch Compressor. *Phys. Rev. Lett.* **124**, 054801 (2020).
31. Zhao, L. et al. Femtosecond Relativistic Electron Beam with Reduced Timing Jitter from THz Driven Beam Compression. *Phys. Rev. Lett.* **124**, 054802 (2020).

Acknowledgements

We wish to acknowledge the technical and scientific teams at the Compact Linear Accelerator for Research and Applications (CLARA) facility for their support and considerable help on all aspects of the operation of the accelerator. We also wish to acknowledge Peter G. Huggard and Mat Beardsley from Rutherford Appleton Laboratory (RAL)-Space for the manufacture of the dielectric-lined waveguide structure and for the provision of a THz Schottky diode used for THz-electron beam synchronisation.

This work was supported by the United Kingdom Science and Technology Facilities Council [grant numbers ST/N00308X/1, ST/N003063/1, ST/P002056/1].

Author contributions

All authors participated in the experiment and contributed to data analysis. M.T.H., D.S.L., D.A.W., V.G., O.J.F. and D.M.G. developed the THz source. A.L.H., G.B. and S.P.J. designed the DLW. A.L.H., E.J.H.S., O.J.F., R.B.A. and S.P.J. modelled the electron energy spectra and performed the longitudinal phase-space calculations. V.G. characterised the DLW and developed the data acquisition software. T.H.P., J.K.J. and Y.S. analysed the beam dynamics of the CLARA accelerator. M.T.H., D.M.G. and S.P.J. wrote the manuscript with contributions from all. E.W.S., R.B.A., G.B., D.M.G. and S.P.J. managed the project.

Additional information

The authors also wish to highlight that since the original submission, recently published works detailing THz-driven compression and timing-jitter reduction of relativistic 3 MeV beams^{30,31} have been added to the reference list for context.

All correspondence should be addressed to S.P.J.

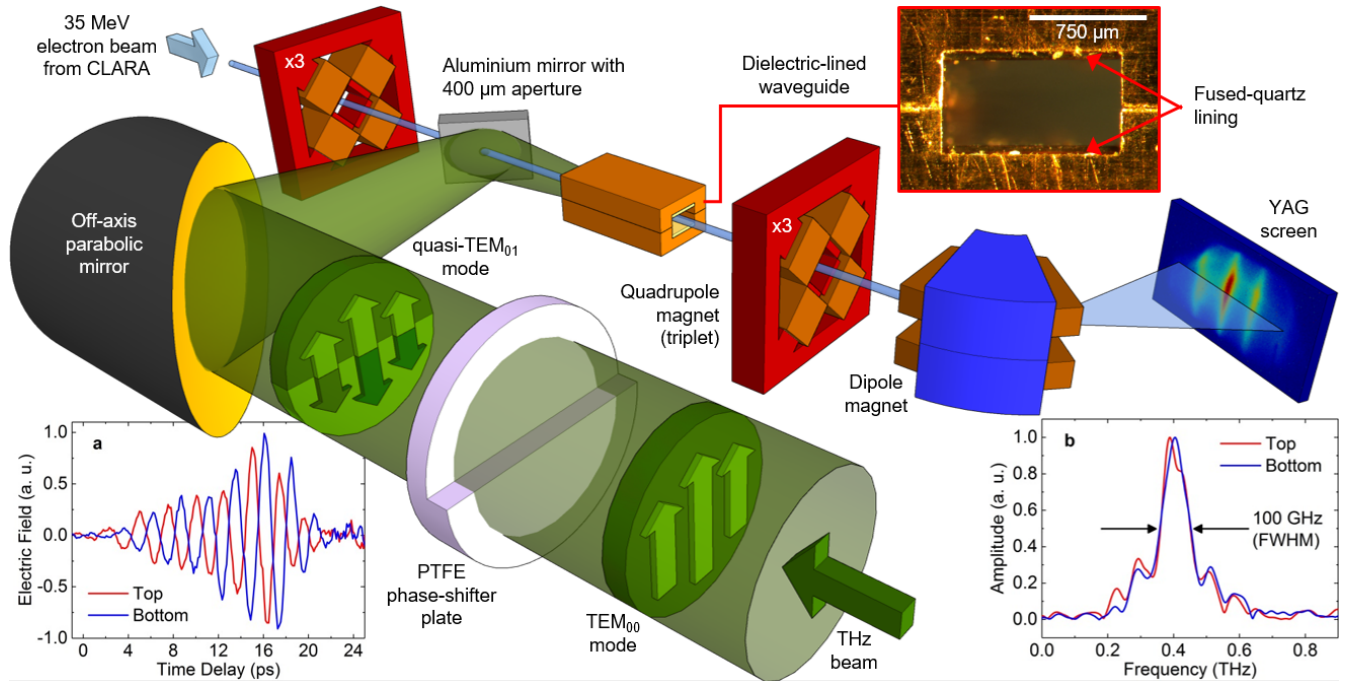


Figure 1: Experimental setup. Schematic diagram showing the THz beam converted into a quasi-TEM₀₁ mode by a PTFE phase-shifter plate and focused into the DLW for collinear interaction with the 35 MeV electron beam. A microscope image of the DLW exit is shown, revealing the dielectric lining along the top and bottom surface. Inset: a,b, Electro-optic sampling measurements of the (a) temporal and (b) spectral profiles of the THz pulse transmitted through the top and bottom half of the phase-shifter plate, recorded at the entrance to the DLW coupling horn.

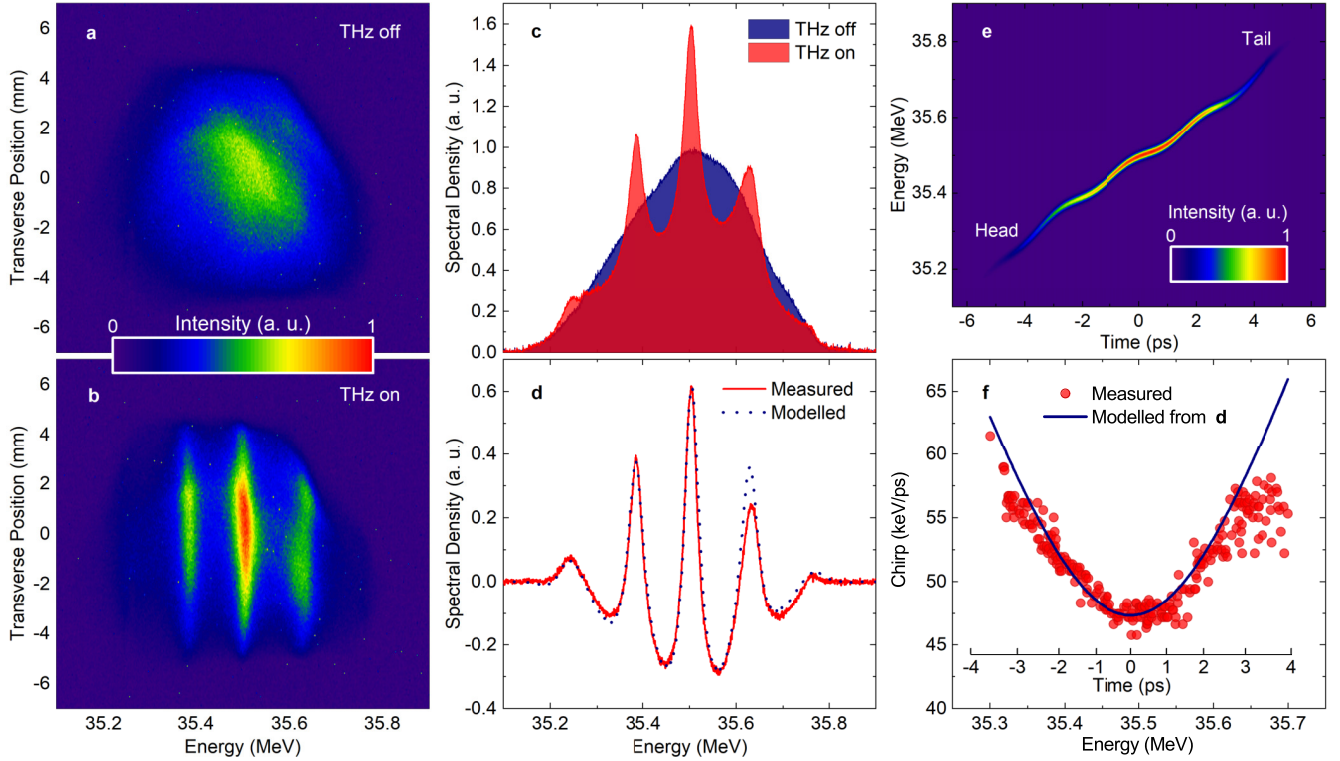


Figure 2: Multi-cycle energy modulation. a,b,c, Single-shot images of the long-duration (6 ps FWHM), high energy spread (330 keV FWHM) electron bunch with (a) THz off, (b) THz on and (c) the corresponding energy density spectra. d, Measured modulation, extracted from the difference between the THz on and THz off spectra in (c), with optimised model indicating a THz-driven peak electron energy gain of 8.8 keV. e, Longitudinal phase-space calculation of the modulated electron bunch. f, Measured chirp as a function of energy obtained from 100 successive THz on shots, shown with the modelled chirp, independently obtained from the modelled modulation in (d).

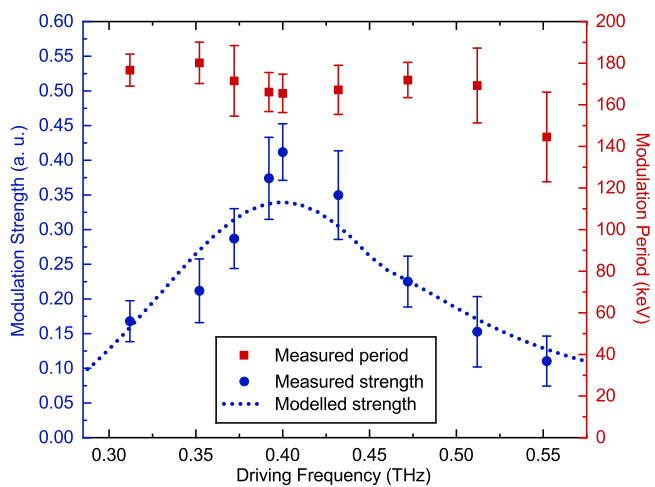


Figure 3: Phase-velocity matching. Measurement of both the modulation strength with supporting model obtained from the calculated DLW dispersion, and modulation period, as a function of THz driving frequency. Error bars represent the standard deviation from 100 individual single-shot measurements. A long-bunch accelerator configuration with increased bunch chirp was used for these measurements.

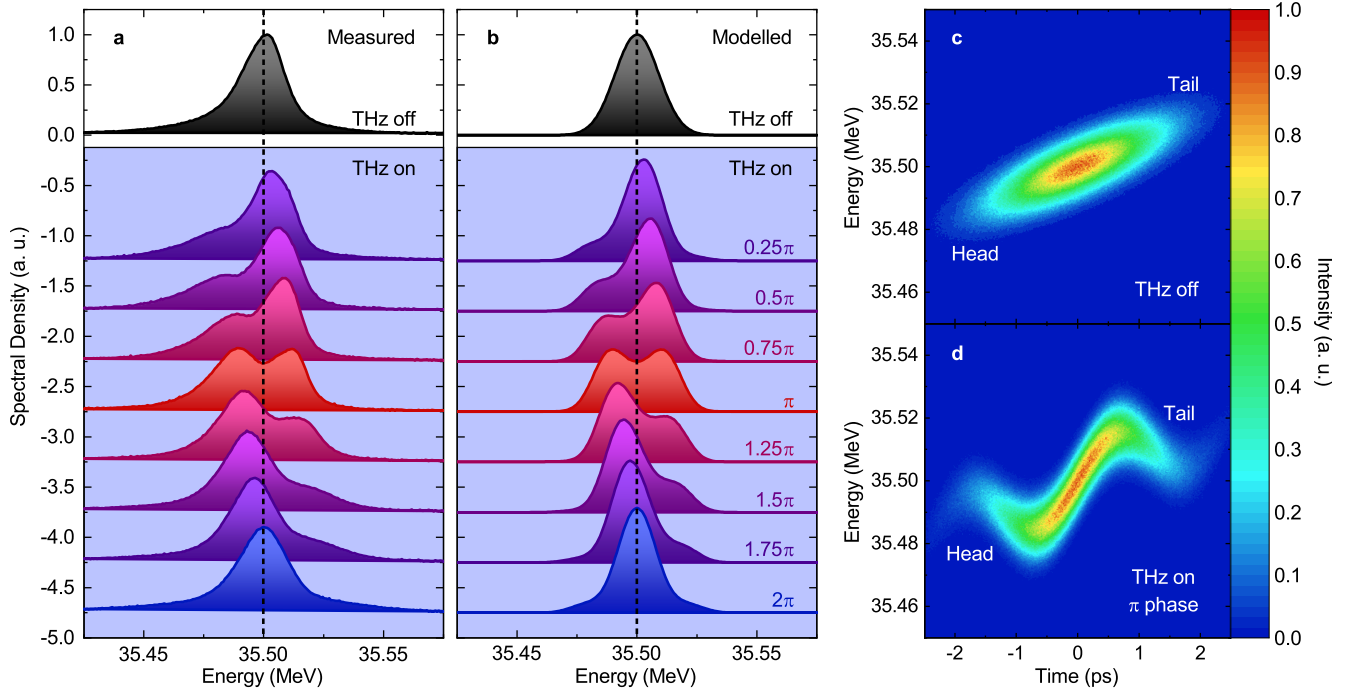


Figure 4: Sub-cycle bunch acceleration. a, Measured single-shot electron energy spectra with THz off and THz on, obtained using short-duration (2 ps FWHM), low energy spread (21 keV FWHM) electron bunches. Due to timing jitter, the phase-ordering was determined from the modelled spectra. b, Modelled electron energy spectra shown at discrete bunch injection phases over the full 2π range of the THz pulse cycle. c,d, Modelled longitudinal phase-space distribution of the electron bunch with (c) THz off and (d) THz on at π injection phase.